



## OPEN ACCESS

## EDITED BY

Dion Dickman,  
University of Southern California,  
United States

## REVIEWED BY

Frederic John Hoerndli,  
Colorado State University, United States  
Peter Juo,  
Tufts University, United States  
C. Andrew Frank,  
The University of Iowa, United States

## \*CORRESPONDENCE

Elva Díaz  
✉ ediaz@ucdavis.edu

RECEIVED 11 November 2024

ACCEPTED 24 December 2024

PUBLISHED 23 January 2025

## CITATION

Specá DJ, He C-W, Meyer CM, Scott EC and Díaz E (2025) Functional characterization of endocytic signals in the SynDIG/PRRT family members SynDIG1 and SynDIG4 in heterologous cells and neurons. *Front. Cell. Neurosci.* 18:1526034. doi: 10.3389/fncel.2024.1526034

## COPYRIGHT

© 2025 Specá, He, Meyer, Scott and Díaz. This is an open-access article distributed under the terms of the [Creative Commons Attribution License \(CC BY\)](https://creativecommons.org/licenses/by/4.0/). The use, distribution or reproduction in other forums is permitted, provided the original author(s) and the copyright owner(s) are credited and that the original publication in this journal is cited, in accordance with accepted academic practice. No use, distribution or reproduction is permitted which does not comply with these terms.

# Functional characterization of endocytic signals in the SynDIG/PRRT family members SynDIG1 and SynDIG4 in heterologous cells and neurons

David J. Specá<sup>1</sup>, Chun-Wei He<sup>1</sup>, Christina M. Meyer<sup>1</sup>, Erin C. Scott<sup>1,2</sup> and Elva Díaz<sup>1\*</sup>

<sup>1</sup>Department of Pharmacology, School of Medicine, University of California, Davis, Davis, CA, United States, <sup>2</sup>Max Planck Florida Institute for Neuroscience, Jupiter, FL, United States

The transmembrane protein Synapse Differentiation Induced Gene 4 (SynDIG4), also known as Proline-rich transmembrane protein 1 (PRRT1), is an AMPA-type glutamate receptor (AMPA) auxiliary factor that is necessary for maintaining extra-synaptic pools of GluA1. Loss of SynDIG4, and the subsequent decrease in extra-synaptic GluA1, has been found to significantly impact synaptic plasticity in the hippocampus. However, how SynDIG4 establishes and maintains these pools is unclear. Previous studies suggested that endocytic machinery is important for maintaining a pool of mobile surface AMPARs, and that proteins associated with such cellular machinery are critical for proper protein trafficking and internalization. Given that SynDIG4 co-localizes with GluA1 in early and recycling endosomes in cultured hippocampal neurons, we sought to identify the sorting signals that target SynDIG4 to endosomes to further elucidate the role of SynDIG4 in GluA1 trafficking. In this study, we report that SynDIG4 possesses a YxxΦ sorting motif, 178-YVPV-181, responsible for binding to the AP-2 complex cargo-sorting subunit μ2. This motif appears critical for proper SynDIG4 internalization, as SynDIG4 mutant 178-AVPA-181, which disrupts binding to μ2, induces aberrant SynDIG4 accumulation at the plasma-membrane of heterologous cells and primary rat hippocampal neurons. We also show that SynDIG4 mutants lacking an endocytic signal co-localize with GluA1 but less so with GluA2 on the surface of heterologous cells. Furthermore, we show that another family member, SynDIG1, is enriched in the trans-Golgi network (TGN) and can traffic between the TGN and plasma membrane. We have identified a non-canonical μ2 binding sequence in SynDIG1 that induces aberrant accumulation at the plasma membrane of heterologous cells and primary rat hippocampal neurons, suggesting a conserved role for μ2-mediated endocytosis within the SynDIG family. These results provide important insight into the mechanisms by which SynDIG proteins are targeted to endosomal compartments as a step in understanding SynDIG-mediated regulation of AMPAR trafficking.

## KEYWORDS

SynDIG1, Capucin, SynDIG4, IFITM3, AP2, GluA1, AMPAR, TGN

## Introduction

The founding member of the *Synapse Differentiation Induced Gene* (*SynDIG*) family of AMPA receptor (AMPA) auxiliary factors was originally identified in a microarray screen for molecules differentially expressed during the period of synapse development in the mouse cerebellum (Díaz et al., 2002). Functional studies of *SynDIG1*, which is also expressed in the hippocampus and throughout the cortex, demonstrated that *SynDIG1* regulates AMPAR content at developing synapses in dissociated rat hippocampal neurons (Kalashnikova et al., 2010). Furthermore, *SynDIG1* was found to positively influence excitatory synapse number when overexpressed in cultured hippocampal neurons. Ultrastructural analysis of hippocampal synapses in mice lacking *SynDIG1* showed a decrease in the number of synapses with a mature phenotype (Chenaux et al., 2016). In a separate study using hippocampal slice preparations, it was demonstrated that while *SynDIG1* did not influence AMPAR biophysical properties, it nonetheless increases both AMPAR and NMDA receptor (NMDAR) content and functional excitatory synapse number when overexpressed (Lovero et al., 2013). Taken together, these studies suggest that *SynDIG1* is involved in excitatory synapse development and maturation. Intriguingly, loss of *SynDIG1* also blocks homeostatic synaptic plasticity in response to tetrodotoxin treatment (Kaur et al., 2016), and indeed it has been shown that *SynDIG1* is phosphorylated in response to treatment with tetrodotoxin (Wu et al., 2022).

In contrast to *SynDIG1*, we found that a related family member, *SynDIG4* does influence biophysical properties of AMPARs in a subunit-dependent manner. Specifically, coexpression of *SynDIG4* with GluA1 or GluA1 + GluA2 in *Xenopus* oocytes slows their deactivation kinetics (Matt et al., 2018), indicating that *SynDIG4* interacts directly with AMPARs. In support of this finding, several studies have identified *SynDIG4* in GluA1-containing AMPAR complexes, including mass spectrometry studies of affinity-purified AMPARs (Shanks et al., 2012; Schwenk et al., 2012; Chen et al., 2014) and cryo-electron microscopy (cryoEM) performed on native AMPARs isolated from mouse brain tissue (Yu et al., 2021). Electrophysiological recordings in hippocampal slices from mice lacking *SynDIG4* reveal deficits in one form of long-term potentiation (1 x 100 Hz tetanus LTP) (Matt et al., 2018) and in long term depression (LTD) (Troyano-Rodriguez et al., 2019). In addition to biophysical changes, there is reduced surface expression of GluA1 and GluA2 in hippocampal lysates (Troyano-Rodriguez et al., 2019) and a striking deficit in extrasynaptic GluA1 and GluA2 in cultured hippocampal neurons from mice lacking *SynDIG4* (Matt et al., 2018), suggesting that *SynDIG4* also plays a role in trafficking or stabilization of AMPARs.

Bioinformatic analysis has revealed that the *SynDIGs* share a distant structural homology with at least 10 other molecules (Sällman Almén et al., 2012), including a family of four molecules named Interferon Inducible Transmembrane proteins (IFITMs), which are involved in the innate immune response (Zhao et al., 2018; Everitt et al., 2012). The larger superfamily was originally designated “Dispanins” because of two predicted helical hydrophobic segments capable of spanning the plasma membrane. However, subsequent studies have shown that they are single-pass type II transmembrane proteins with internal N-termini and extracellular C-termini (Kalashnikova et al., 2010; Kirk et al., 2016;

Ling et al., 2016; Martin et al., 2021; Weston et al., 2014). The first helix, rather than spanning the membrane, may be buried in the membrane, and in the case of IFITM3, this helix has amphipathic character which may associate with the inner leaflet of the plasma membrane (Ling et al., 2016; Chesarino et al., 2017). In addition to the shared topology, dispanin family members share two conserved cysteine residues which can be reversibly palmitoylated (Kaur et al., 2016; Yount et al., 2010; Yount et al., 2012). It has been proposed that the function of this family of molecules is to act as “fusogens” by either promoting or inhibiting membrane fusion (Coomer et al., 2021).

IFITM3 is trafficked transiently to the plasma membrane but rapidly endocytosed and transported to the endolysosomal network, where it acts to restrict viral entry, perhaps by inhibiting the formation of a fusion pore (Spence et al., 2019; Desai et al., 2014). IFITM3 harbors an endocytic signal which interacts with the  $\mu 2$  subunit of the multi-subunit Adaptor Complex, AP2 (Jia et al., 2014; Chesarino et al., 2014). This complex forms a bridge between cargo and clathrin and is critical for clathrin-mediated endocytosis (Bonifacino and Traub, 2003). Mutation of this endocytic signal disrupts the interaction with  $\mu 2$ , resulting in accumulation of IFITM3 on the plasma membrane and an alteration in the ability of IFITM3 to restrict viral entry (Jia et al., 2014; Chesarino et al., 2014).

This work inspired us to explore whether the *SynDIGs* also harbor endocytic signals which could interact with  $\mu 2$  and the  $\mu$  subunits of other adaptor complexes which are involved in many different intracellular trafficking pathways (Guardia et al., 2018). A better understanding of the trafficking of the *SynDIGs* might provide greater insight into how *SynDIG4* and *SynDIG1* can influence AMPAR trafficking and synapse development.

## Materials and methods

### Animals and neuronal culture

All animal use was approved by the institutional animal care and use committee at the University of California, Davis, in accord with the guidelines laid out by the US Public Health Service. For rat cultures, hippocampal neurons were dissected from wild-type E18 Sprague Dawley rat pups of both sexes and plated in 6-well plates at a density of 150,000 cells per well. For mouse cultures, hippocampal neurons were dissected from wild-type P0 C57BL/6J mouse pups of both sexes and plated in 6-well plates at a density of 100,000 cells per well. Cells from both cultures were maintained in wild-type rat-derived astrocyte-conditioned neuron maintenance medium (NMM) consisting of 1X Neurobasal (NB) medium (Gibco #21103049), 1X GlutaMAX (Gibco #35050061), and 1X B-27 supplement (Gibco #17504044). Rat cultures were transfected with the indicated plasmids using the subsequently detailed protocol between 5 and 9 days *in vitro* (DIV). Mouse cultures were transfected with the indicated plasmids using the same protocol at DIV9.

For transfection, NB medium was equilibrated in the incubator for at least 1 h. Then, the coverslips were transferred into the equilibrated NB. Concurrently, 1.5  $\mu$ g of DNA in 50  $\mu$ L of NB was mixed with 2.5  $\mu$ L of Lipofectamine 2000 (Invitrogen #11668027) in 50  $\mu$ L of NB. This mixture was incubated at room temperature (RT) for 35 to 60 min. The Lipofectamine:DNA mix was then added to the

neurons and allowed to incubate in a 37°C incubator for 1 h before being transferred back to the astrocyte-conditioned NMM.

For rat cultures, DIV18 ~ 22 hippocampal cultures were fixed with 4% paraformaldehyde (PFA) and 4% sucrose in PBS for 5 min at RT. Coverslips were washed once with cold PBS followed by blocking with 5% fetal bovine serum in PBS (blocking solution) at RT for 2 h. The neurons were stained with the anti-HA antibody (Cell Signaling Technology Cat# 3724, RRID: AB\_1549585) at RT. After 2 h, the neurons were then washed three times with PBS, followed by permeabilization with 0.25% Triton X-100 at RT for 8 min. Coverslips were washed with PBST (0.01% Triton in PBS) and incubated with blocking solution at RT for 2 h. The antibodies against PSD95 (UC Davis/NIH NeuroMab Facility Cat# K28/43, RRID: AB\_2877189) and FLAG (Sigma-Aldrich Cat# F3165, RRID: AB\_259529) were added to the neurons at 4°C overnight. After washing three times with PBST, coverslips were incubated in blocking solution at RT for 2 h and fluorophore-conjugated secondary antibodies were applied to the coverslips for 2 h at RT.

For mouse cultures, DIV18 hippocampal cultures were live-fed the previously listed anti-Flag antibody for 10 min at RT, followed by a 10-min incubation of the secondary antibody (Invitrogen Goat anti-Mouse IgG1 Alex Fluor 647 Cat#A-21240; RRID: AB\_2535809). Cultures were then fixed with 4% PFA and 4% sucrose in PBS for 10 min at RT, followed by three washes in RT PBS. All subsequent steps follow the rat culture protocol, with the difference being that anti-myc (Cell Signaling Cat#9B11, RRID: AB\_331783) and MAP2 (Millipore Cat#AB5622-I, RRID: AB\_2800501) antibodies were added to neurons at 4°C overnight.

## Plasmids

Epitope tags were added, or amino acid substitution mutations were made to cDNAs from mouse SynDIG1, mouse SynDIG2 or rat SynDIG4 using a Q5<sup>®</sup> Site-directed mutagenesis kit (NEB Cat#E0554S). For N-terminal tags, a methionine codon was added to the 5' end of the sequence encoding the epitope tag and the original methionine start codon was replaced with this sequence. For C-terminal epitope tags, the epitope tag sequence was inserted directly after the final codon. For C-terminally tagged SynDIG1-Flag and associated deletion mutants, a flexible linker was added to facilitate proper expression (sequence: GGSGGDYKDDDDK). Information on all constructs used in this study are described in greater detail in [Supplementary Table 1](#).

## Cell culture

All cell lines were grown in a humidified incubator at 37°C and 5% CO<sub>2</sub>. COS-7 cells (ATCC Cat# CRL-1651, RRID: CVCL\_0224) and HEK293T cells (ATCC Cat# CRL-3216) were maintained in Dulbecco's modified Eagle's medium (Gibco Cat # 11995-065) supplemented with 10% fetal bovine serum (Avantor Seradigm Cat#97068-085) and 1% penicillin/streptomycin.

## Co-immunoprecipitation

For co-immunoprecipitation studies, HEK293T cells were used because of their robust transfection and transient expression

ability. On day one, 170,000 cells/well were seeded into 6 well plates. On day three, confluent cells were transfected for 4 h with 2.5 μg DNA/well (500 ng SynDIG +2,000 ng μAP subunit or pcDNA3.1 empty vector) using Lipofectamine 2000 (ThermoFisher Cat# 11668027), and cells were allowed to express the constructs for >24 h. On day four, co-immunoprecipitation was performed using an α-HA magnetic bead immunoprecipitation (IP) kit (ThermoFisher Cat# 88838) following the manufacturer's protocol. In brief, cells were rinsed twice with ice cold phosphate-buffered saline (PBS) containing 1 mM CaCl<sub>2</sub>, 0.5 mM MgCl<sub>2</sub> and solubilized with 500 μL IP wash buffer/well (including protease inhibitors and PMSF) for 90 min at 4°C with rotation. Lysates from two wells were combined for each replicate (1,000 μL total). Nuclei and insoluble material were pelleted with centrifugation at >13,000xg for 15 min at 4°C. 80 μL of solubilized protein was reserved as input, while 800 μL of supernatant was added to 30 μL α-HA magnetic beads and incubated for 90 min at RT with rotation. Beads were then washed three times with IP wash buffer, once with double-distilled H<sub>2</sub>O and then eluted with 100 μL non-reducing sample buffer (NRSB). Dithiothreitol (DTT, 50 mM) was added following elution.

## Immunoblotting

Input (15 μL) and IP (50 μL) protein samples were heated to 70°C for 10 min and separated via gel electrophoresis on a Bio-Rad minigel system using 4–20% gradient gels (Bio-Rad Cat# 456-1,094). Following separation and transfer to nitrocellulose, membranes were blocked with 4% milk in Tris-buffered saline (TBS) with 0.1% Tween-20 (TBST) for 60 min at RT. Membranes were then incubated overnight at 4°C with the following primary antibodies in 4% TBST: Mouse α-myc IgG2a (Cell Signaling Technology Cat# 2276, RRID:AB\_331783, 1:1,000), Rat α-HA (Roche Cat# 11867423001, RRID:AB\_390918, 1:500, for use on input samples) or Rabbit α-HA (Cell Signaling Technology Cat# 3724, RRID:AB\_1549585, 1:1,000, for use on IP samples). The following day, membranes were washed three times with TBST and incubated with the following secondary antibodies: Goat α-mouse Azure 700 (Azure Biosystems Cat# AC2129, RRID:AB\_3331665, 1:1,000) and Goat α-Rat H + L Alexa 488 (Jackson ImmunoResearch Labs Cat# 112-545-167, RRID:AB\_2338362; 1:500, for use on input samples) or Goat α-Rabbit Alexa 790 (Jackson ImmunoResearch Labs Cat# 111-655-144, RRID:AB\_2338086; 1:500, or use on IP samples). Membranes were washed three times with TBST and once with TBS prior to imaging.

## Imaging and quantification of immunoblots

Fluorescent immunoblot images were acquired on a Sapphire Bioimager (Azure Biosystems Model #Sapphire RGBNIR) and quantified with Azure spot software (ver 2.0). For analysis, the amount of eluted interacting protein (in most cases, a myc-tagged SynDIG construct) was normalized to both the amount of eluted interacting protein (in most cases, an HA-tagged μ2 subunit) and to the amount of input interacting protein (in most cases, a myc-tagged SynDIG construct).

## Immunofluorescence immunocytochemistry

For immunocytochemistry experiments, COS7 cells were used to better visualize intracellular organelles. For each experiment, 30,000 cells/well were seeded onto coverslips coated with collagen in 6 well tissue culture plates. The following day, nonconfluent cells were transfected for 4 h with 1  $\mu$ g DNA (250 ng SynDIG +750 ng empty vector) using Lipofectamine 2000. The following day, transfected cells were fixed and stained; however, prior to fixation, the following procedures were used: for live **surface labeling** experiments, cells were rinsed twice with ice cold PBS (containing 1 mM CaCl<sub>2</sub>, 0.5 mM MgCl<sub>2</sub>) and then blocked for 20 min with prechilled 0.2% bovine serum albumin (BSA) in PBS at 4°C. Cells were then incubated for 20 min with primary antibodies [either Mouse  $\alpha$ -myc IgG2a (Cell Signaling Technology Cat# 2276, RRID:AB\_331783, 1:1,000), Rat  $\alpha$ -HA (Roche Cat# 11867423001, RRID:AB\_390918, 1:200), or Ms.  $\alpha$ -Flag (Sigma-Aldrich Cat# F3165, RRID: AB\_259529; 1:500)], followed by three BSA-PBS washes and incubation with appropriate secondary antibodies. For **antibody feeding** experiments, myc-SynDIG1-Flag transfected cells were incubated with  $\alpha$ -Flag antibody at 37°C for 60 min. For **steady state localization** experiments, cycloheximide (100  $\mu$ M) was added to the media for four hours prior to fixation at 37°C to inhibit protein translation.

Regardless of treatment, all cells were then rinsed three times with ice cold PBS (+1 mM CaCl<sub>2</sub>, 0.5 mM MgCl<sub>2</sub>) and fixed with prechilled 3% glyoxal solution (Richter et al., 2018) for 30 min at RT, followed by one rinse with PBS, quenching with ammonium chloride (50 mM) for 15 min, permeabilization with 0.1% Triton X-100 and blocking with BSA for 60 min (all diluted in PBS). Cells were incubated overnight at 4°C with primary antibodies to Golgin-97 (Cell Signaling Technology Cat# 13192, RRID: AB\_2798144, 1:100), EEA1 (BD Biosciences Cat# 610456, RRID: AB\_397829; 1:250), GM130 (BD Biosciences Cat# 610822, RRID: AB\_398141; 1:500), and  $\alpha$ -myc or  $\alpha$ -HA antibodies noted above.

## Confocal imaging and analysis

Images were acquired on a Leica SP8 instrument in confocal mode with a 63x objective and z stack images were taken through the entire cell volume. Image analysis was performed using FIJI/ImageJ (ver. 2.14.0/1.54f). For determination of surface expression, we analyzed maximum projections. Regions of interest (ROI) were drawn manually around the border of individual cells and integrated density (using a uniform threshold determined for each channel) was measured for both surface and total expression and used to generate a ratio. The SynDIG2 constructs only had a C-terminal HA tag. The total stain integrated density for the SynDIG2 $\Delta$ 135–55 deletion mutant was very low, perhaps because the HA epitope recognized by the  $\alpha$ -HA antibody used for labeling total protein was blocked by the  $\alpha$ -HA antibody used for surface staining. This led to unrealistically high surface/total ratios. To produce a more realistic value for total stain, we added surface+total to create a total stain value to be used as the denominator. To calculate Manders Correlation Coefficients (MCC), we used JaCoP plugin, using manually determined thresholds.

For MCC calculations to improve resolution of GM130 and Golgin-97, zoomed in images were acquired and deconvoluted using Huygens Software (Scientific Volume Imaging), and a single z slice was used for analysis. For analysis of SynDIG4 overlap with surface AMPARs, to improve resolution, images were deconvoluted and maximum projections of surface staining were used for analysis. In this situation a uniform square ROI was centered over the cell to avoid cell edges which tended to have artefactual staining.

## Statistics

Statistical analysis was performed using GraphPad Prism (ver. 10.3.1). In experiments where two groups were compared, we used an unpaired *t*-test, except for the calculation of GM130 and Golgin-97 co-localization where we used a paired *t*-test. In experiments comparing three or more groups, if the variance was not significantly different, we used a one-way ANOVA with post-hoc Tukey test. If the variance was significantly different, we used a Brown-Forsythe ANOVA with post-hoc Dunnett's test.

## Results

### SynDIGs associate with $\mu$ AP subunits

Inspired by research into the endocytic trafficking of IFITM3 mediated by an interaction with the  $\mu$ 2 AP subunit (Jia et al., 2014; Chesarino et al., 2014), we performed co-immunoprecipitation experiments in HEK293T cells with several SynDIG proteins: SynDIG1 (also known as Tmem90b), the closely related SynDIG2 (also known as SynDIG1L, Tmem90a, or capucin) and SynDIG4 (also known as Prrt1 or NG5) (Figure 1). We used IFITM3 as a positive control for interaction with  $\mu$ 2 and surveyed multiple  $\mu$ AP subunits, including  $\mu$ 1a,  $\mu$ 2,  $\mu$ 3a and  $\mu$ 4. We confirmed that IFITM3 co-immunoprecipitates robustly with  $\mu$ 2 as previously reported (Jia et al., 2014), but we also detected weaker interactions with  $\mu$ 1a and  $\mu$ 4. We found that SynDIG1 interacted strongly with  $\mu$ 2 and to a lesser extent with  $\mu$ 1a. SynDIG4 was differentially co-immunoprecipitated by all four  $\mu$ AP subunits, while SynDIG2 did not appear to interact with  $\mu$ 2 or any  $\mu$ AP subunit, despite being closely related to SynDIG1 (43% identity, 53% similarity) (Figure 1B). We searched for canonical endocytic signals including tyrosine-based YXX $\phi$  ( $\phi$  being a bulky hydrophobic amino acid) or dileucine-based motifs (Bonifacino and Traub, 2003). We found no canonical signals in SynDIG1; however, several large deletions of the intracellular domain led us to focus on amino acids 144–180 (C-W.H. & D.J.S., unpublished observations) (Figure 1A), and we made three deletion mutants within this critical region for co-immunoprecipitation and further studies. We found that deletion of amino acids 161–76 eliminated almost all binding to  $\mu$ 2 ( $F = 127.5$ ,  $p < 0.0001$ ) (Figure 1C). Interestingly, a smaller deletion of residues 161–72 still retains binding to  $\mu$ 2 when normalized for its lower total expression, suggesting that amino acids 173-FLMM-176 could be a noncanonical endocytic signal with a phenylalanine residue instead of a tyrosine. Furthermore, we observed significantly decreased binding of the 161–76 deletion to the  $\mu$ 1a subunit (Figure 1C).

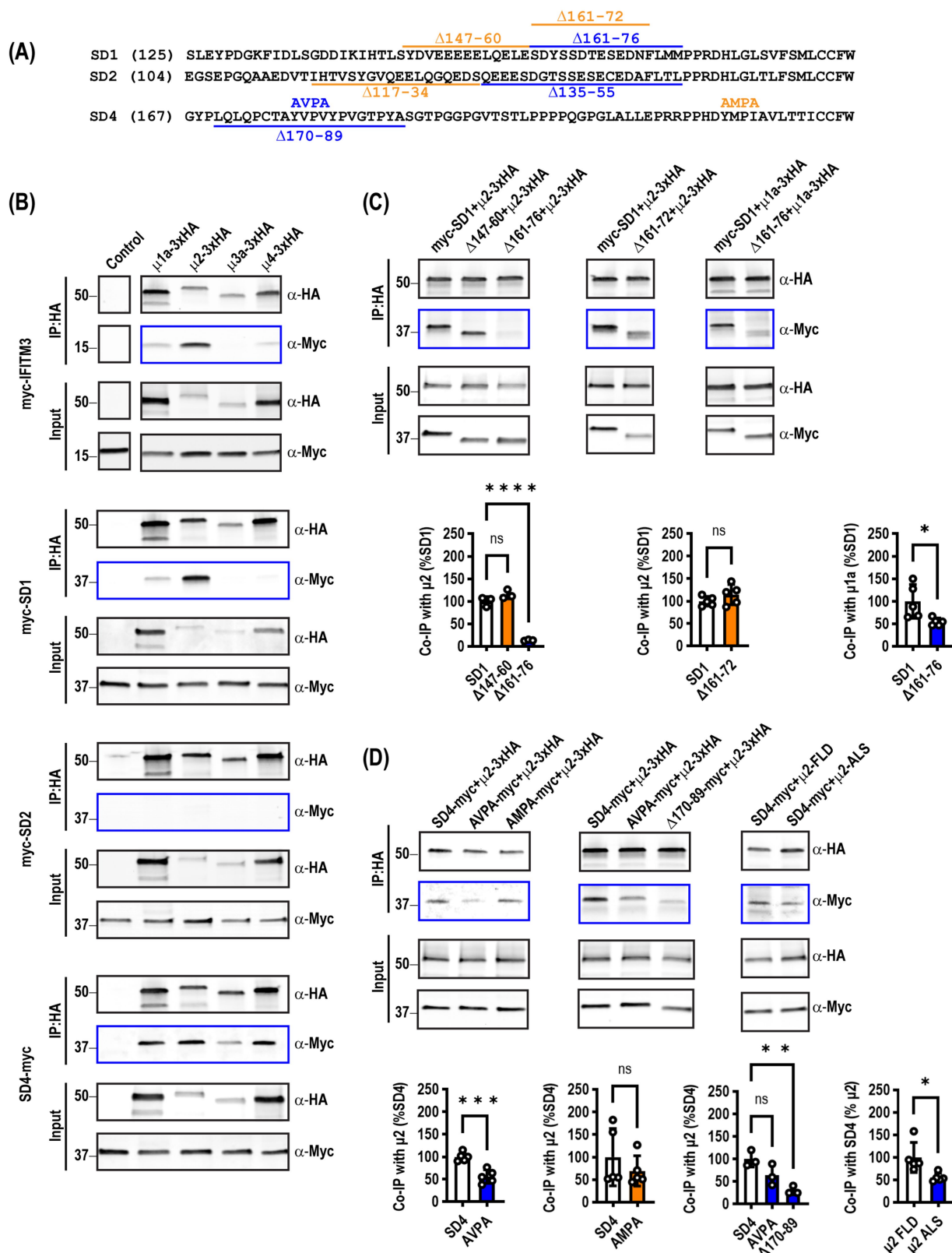


**FIGURE 1**  
SynDIG1 and SynDIG4 co-immunoprecipitate with the μ2 AP subunit. HA-tagged μAP subunits were used to co-immunoprecipitate myc-tagged SynDIG constructs expressed in HEK293T cells. **(A)** Schematic diagram of SynDIG deletion mutants used in this study. Number in parentheses indicates position of the leftmost amino acid. Constructs highlighted in blue disrupted the interaction with μ2 and/or influenced surface expression whereas constructs highlighted in orange did not. **(B)** Representative survey of interactions between μAP subunits and SynDIGs. **(C)** Representative images and quantification of interactions between SynDIG1 and μ2 and μ1a. **(D)** Representative images and quantification of interactions between SynDIG4 and μ2.

(Continued)

## FIGURE 1 (Continued)

To calculate co-immunoprecipitation values, the amount of SynDIG protein immunoprecipitated was divided by the amount of  $\mu$  protein immunoprecipitated and then normalized to the amount of SynDIG protein in the input. The mean value of all the control samples was then used to normalize all the values within a given experiment. Data are represented as mean  $\pm$  SEM;  $n = 3$ –5 biological replicates per group; ns, not significant. \* $p < 0.05$ ; \*\* $p < 0.01$ ; \*\*\* $p < 0.001$ ; \*\*\*\* $p < 0.0001$ .

The intracellular portion of SynDIG4 has two potential YXX $\phi$  signals, 178-YVPV-181 and 223-YMPI-226 (Figure 1A). We made alanine substitution mutants (YVPV $\rightarrow$ AVPA and YMPI $\rightarrow$ AMPA) to test for co-immunoprecipitation with  $\mu 2$ . We found that the YVPV $\rightarrow$ AVPA mutant significantly decreased the interaction with  $\mu 2$  while the YMPI $\rightarrow$ AMPA did not; however, it was clear that the interaction was not eliminated completely. Therefore, we made a deletion mutation of amino acids surrounding the YXX $\phi$  signal, and this further decreases the interaction ( $F = 11.38$ ,  $p = 0.0091$ ) (Figure 1D). The crystal structures of  $\mu$  subunits reveal critical conserved amino acids that bind to the tyrosine residue in the YXX $\phi$  signal (Heldwein et al., 2004; Owen and Evans, 1998). We mutated two of these residues (FLD  $\rightarrow$  ALS) and showed that less SynDIG4 protein is co-immunoprecipitated with the  $\mu 2$  ALS mutant, suggesting that the SynDIG4 signal is binding in the same pocket (Figure 1D).

### Mutation of $\mu 2$ AP binding sites in SynDIGs increases surface expression

The same deletion constructs tested for their ability to co-immunoprecipitate with  $\mu 2$  were transfected into COS7 cells to determine whether mutants that disrupted an interaction with  $\mu 2$  resulted in increased accumulation of SynDIGs on the plasma membrane, as would be expected when endocytosis is disrupted. Cells were live labeled on ice with appropriate primary and secondary antibodies to recognize an extracellular epitope tag, then fixed and stained for total expression of the same molecule. For SynDIG1, we observed very little wild type (WT) protein expressed on the surface, but there was a significant increase in surface expression of the 161–76 deletion mutant that eliminates the interaction with  $\mu 2$  ( $F = 20.97$ ,  $p < 0.0001$ ) (Figure 2A).

Although we did not detect an interaction between  $\mu 2$  and SynDIG2, we included several deletion mutants in our surface expression studies for comparison. This was done in part to exploit the high conservation between SynDIG1 and SynDIG2 to map the noncanonical endocytic signal in SynDIG1 (Figure 1A). Like SynDIG1, we observed very little surface expression of WT SynDIG2; however, to our surprise, we observed a significant increase in surface expression of the SynDIG2 135–55 deletion mutant, which is roughly equivalent to the SynDIG1 161–76 deletion mutant ( $F = 549.8$ ,  $p < 0.0001$ ) (Figure 2B). This suggests that SynDIG2 has the capability to traffic to the plasma membrane, but that accumulation on the cell surface does not depend on a disruption in binding to  $\mu 2$ . We propose several possible explanations in the discussion section.

We quantified surface expression of WT SynDIG4 and the two endocytic mutants and found a significant increase in AVPA surface expression relative to WT, as we hypothesized, but we also observed decreased surface expression of the AMPA mutant relative to WT ( $F = 27.82$ ,  $p < 0.0001$ ) (Figure 2C). This could be due to a defect in protein folding. Alternatively, it is possible

that the AMPA mutant disrupts binding to another  $\mu$  protein such as  $\mu 1a$ , which could interfere with forward trafficking. In an independent experiment, we confirmed that the SynDIG4 170–89 deletion mutant accumulates on the plasma membrane (Figure 2D).

### SynDIG1 and SynDIG2 expression is enriched in the trans-Golgi network (TGN) and traffic between the plasma membrane, early endosomes and the TGN in COS7 cells

Previous studies indicated that SynDIG2—also named capucin because of its pronounced expression within the caudate putamen—is localized to the cis-Golgi when transiently expressed in HeLa or CHO tissue culture cells (de Chaldée et al., 2006). We reproduced this finding in transiently transfected COS7 cells that were allowed to express for >24 h followed by the addition of 100  $\mu$ M cycloheximide for 4 h to inhibit protein translation to investigate steady state localization of both SynDIG2 and SynDIG1. We also observed an enrichment in the Golgi; however, when we quantified the colocalization of SynDIG1 and SynDIG2 with cis-Golgi (GM130) and trans-Golgi (Golgin-97) markers, we observed a highly statistically significant enrichment of both proteins in the TGN as opposed to the cis-Golgi (Figure 3A).

We performed the same cycloheximide-based steady state analysis with the SynDIG1 and SynDIG2 deletion mutants. In both cases, we observed a statistically significant decrease in the correlation coefficient between the TGN marker and the deletion mutants which accumulate at the plasma membrane, compared to WT (SynDIG1:  $F = 22.5$ ,  $p < 0.0001$ ; SynDIG2:  $F = 19.37$ ,  $p < 0.0001$ ). We also quantified correlation coefficients for the early endosome marker EEA1 with these same molecules, demonstrating that at steady state, these molecules are also localized with early endosomes (Figures 3B,C). SynDIG4 and IFITM3 do not localize to the TGN under steady state conditions, rather they both localize to early endosomes and lysosomes (D.J.S., unpublished observations).

To investigate whether WT SynDIG1 can traffic to the plasma membrane transiently, be endocytosed, and then be returned to the TGN, we performed an antibody feeding experiment. We incubated transfected cells with primary  $\alpha$ -Flag antibody for 1 h at 37°C, then washed, fixed and stained for Golgin-97 and labelled with secondary antibodies. We quantified the integrated density of the  $\alpha$ -Flag signal that overlaps with Golgin-97 and determined there was a highly significant increase in signal relative to mock transfected cells, which had very little internalized signal (Figure 3D).

Taken together, these data suggest that SynDIG1 and perhaps also SynDIG2 are enriched in the TGN and can be transported to the plasma membrane where they are rapidly endocytosed and trafficked back to the TGN, although other trafficking pathways are possible.

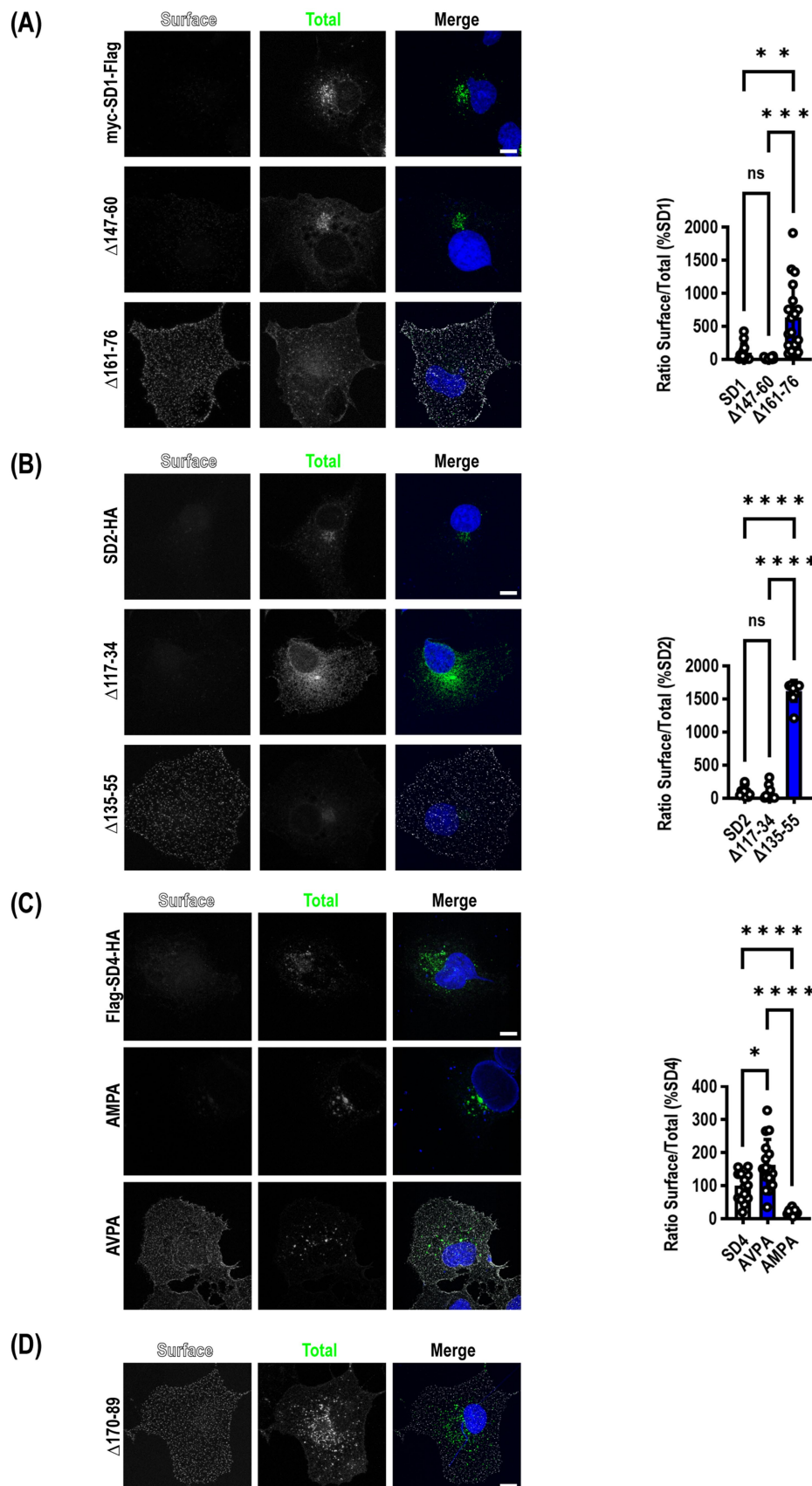


**FIGURE 2** Mutation of  $\mu 2AP$  binding sites in SynDIGs increases surface expression. SynDIG constructs with C-terminal extracellular epitope tags were expressed in COS7 cells and surface labelled. **(A)** Representative images and quantification of surface expression of SynDIG1 and mutants. **(B)** Representative

(Continued)

FIGURE 2 (Continued)

images and quantification of surface expression of SynDIG2 and mutants. (C) Representative images and quantification of surface expression of SynDIG4 and mutants. (D) Representative image of SynDIG4 $\Delta$ 170–89 deletion mutant. Data are represented as mean  $\pm$  SEM;  $n = 13$ –20 cells per group (A);  $n = 10$  cells per group (B);  $n = 13$ –16 cells per group (C), each group from 2 to 3 independent experiments; ns not significant; \* $p < 0.05$ ; \*\* $p < 0.01$ ; \*\*\* $p < 0.001$ ; \*\*\*\* $p < 0.0001$ . Scale bar: 10  $\mu$ m.

## An endocytosis defective SynDIG4 mutant co-localizes with GluA1 at the plasma membrane in COS7 cells

Previously, we have shown that co-transfection of WT SynDIG4 with GluA1 can increase the size of GluA1 clusters in COS7 cells (Plambeck et al., 2022). However, because very little SynDIG4 is present on the plasma membrane, these clusters are not located on the cell surface. In fact, they only occur when surface HA-GluA1 is labelled with primary antibody and then incubated at 37°C for 20–30 min, allowing the receptor to internalize. A similar increase in cluster size is also observed when SynDIG4 is co-transfected with GluA2, but not when co-transfected with GluK2 (Plambeck et al., 2022).

Our endocytosis deficient SynDIG4 mutants enabled us to ask a slightly different question: does SynDIG4 co-localize with ionotropic glutamate receptors at the surface of the plasma membrane? We co-transfected SynDIG4 $\Delta$ 170–89-myc with either HA-GluA1 (flip), HA-GluA2, or HA-GluK2 and live surface labelled both molecules. We found that there was a significantly higher Manders correlation coefficient (MCC) between SynDIG4 and GluA1 than either GluA2 or GluK2 ( $F = 16.02$ ,  $p < 0.0001$ ) (Figures 4A,B). We calculated the surface area of the puncta and observed no difference in SynDIG4 when co-expressed with each receptor (Figure 4C); however, GluK2 was expressed at a consistently higher level than GluA1 or GluA2 (Figure 4D). We rotated the SynDIG4 channel to randomize the data and recalculated the MCC (Figure 4E) and found a significantly higher MCC for GluK2, which was likely driven by its higher expression. Comparing native versus rotated (randomized) MCC analysis between SynDIG4 and GluR constructs, we observed a highly significant difference for GluA1, a significant difference for GluA2 and no difference for GluK2 (Figure 4F).

We were somewhat surprised, based on our previous findings, that GluA2 did not demonstrate a higher correlation coefficient. It is possible that SynDIG4 does not co-localize with GluA2 at the plasma membrane, but it is important to note that the construct used for this experiment lacked 20 amino acids which could be important for mediating interactions with other molecules, including GluA2.

## Endocytosis defective SynDIG mutations promote increased surface expression in cultured hippocampal neurons

We then aimed to assess the role of  $\mu$ 2-dependent SynDIG trafficking within neurons. We transfected mouse dissociated hippocampal neurons at DIV9 with myc-SynDIG1 (WT)-Flag or myc-SynDIG1 ( $\Delta$ 161–76)-Flag constructs and visualized surface and total SynDIG1 using anti-Flag and anti-myc antibodies, respectively, at DIV18. Like our findings in COS cells, overexpression of SynDIG1 $\Delta$ 161–76 resulted in an increased surface to total SynDIG1 ratio compared to WT SynDIG1 (Figure 5A). This result further

suggests that the SynDIG1- $\mu$ 2 binding interaction is required for proper endocytosis in neurons and is mediated by a non-canonical endocytic signal.

We conducted similar experiments within rat dissociated hippocampal neurons for SynDIG4 and its  $\mu$ 2-binding impaired mutation, SynDIG4-AVPA. Flag-SynDIG4 (WT)-HA and Flag-AVPA-HA were transfected into rat dissociated hippocampal neurons at DIV0 and visualized at DIV18–22; similarly, anti-HA and anti-Flag antibodies were utilized to compare the surface to total SynDIG4, respectively. Once again, consistent with our results in COS cells, overexpression of AVPA resulted in a higher surface to total ratio of SynDIG4 compared to WT SynDIG4 (Figure 5B). This result also suggests that SynDIG4- $\mu$ 2 binding is both required for proper endocytosis in neurons and specifically mediated by a canonical YXX $\phi$  signal. Furthermore, AVPA surface puncta were larger than WT SynDIG4 surface puncta, while PSD95 puncta size did not differ between the AVPA and WT SynDIG4 groups (Figure 5C). This result suggests that impaired endocytosis causes SynDIG4 to accumulate on the plasma membrane without affecting the distribution of PSD95. Interestingly, we observed that more PSD95 puncta co-localized with surface AVPA compared to WT SynDIG4, which is primarily found at extrasynaptic sites (Figure 5C). We conclude that the defective endocytosis of AVPA promotes its retention at synapses.

## Discussion

### SynDIG4 colocalizes with GluA1 at the plasma membrane in COS7 cells

We have shown that SynDIG4 has a canonical YXX $\phi$  endocytic signal, and that mutation of this signal disrupts interaction with the  $\mu$ 2 subunit of the AP2 complex, presumably hampering clathrin-mediated endocytosis of SynDIG4 and resulting in its accumulation on the surface of the cell. In transfected heterologous cells, there is almost no observable surface expression of WT SynDIG4 (Figure 2), likely due to rapid endocytosis. The surface localization of the mutant SynDIG4 enabled us to visualize co-localization of SynDIG4 and ionotropic glutamate receptors on the surface of transfected cells (Figure 4). We determined that there is a significantly higher correlation coefficient between SynDIG4 + GluA1 puncta than either SynDIG4 + GluK2 or SynDIG4 + GluA2 puncta. Compared to randomized data, there was also a small but significant difference in SynDIG4 + GluA2 puncta. However, we observed a highly significant difference for GluA1 and no difference for GluK2, suggesting that the correlation coefficient for SynDIG4 + GluA1 is unlikely due to chance and therefore biologically relevant. Whether the preference for SynDIG4 + GluA1 at the cell surface in heterologous cells translates into SynDIG4-mediated regulation of GluA1-containing AMPARs in neurons requires additional experiments beyond the scope of the present study.



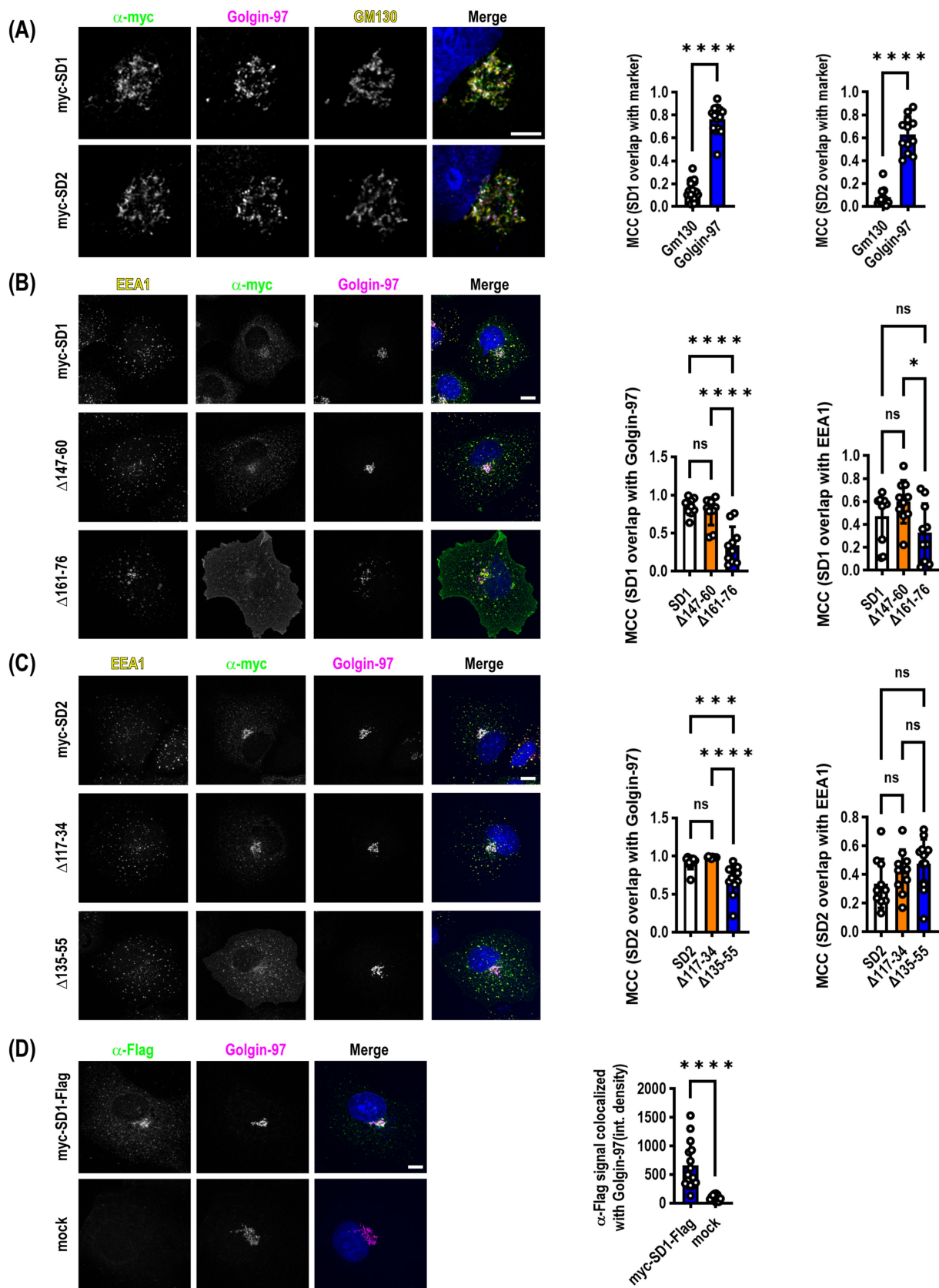


**FIGURE 3**  
 SynDIG1 and SynDIG2 are enriched in the trans-Golgi network. SynDIGs were transiently transfected into COS7 cells to investigate steady state localization after cycloheximide-mediated protein synthesis inhibition. **(A)** Representative images and quantification of SynDIG1 and SynDIG2 co-localization with cis- (GM130) and trans-Golgi (Golgin-97) markers. **(B)** Representative images and quantification of colocalization of SynDIG1 mutants

(Continued)

## FIGURE 3 (Continued)

with Golgin-97 and EEA1. (C) Representative images and quantification of colocalization of SynDIG2 mutants with Golgin-97 and EEA1. (D) SynDIG1 transfected cells (without cycloheximide treatment) were incubated with  $\alpha$ -Flag antibody for 1 h at 37°C to assess trafficking from the plasma membrane to the TGN. MCC, Manders Correlation Coefficient. Data are represented as mean  $\pm$  SEM;  $n = 14$  cells for SynDIG1;  $n = 13$  cells for SynDIG2 (A);  $n = 10$  cells per group (B);  $n = 10$ –13 cells per group (C);  $n = 12$ –15 cells per group (D), each group from 2–3 independent experiments; ns not significant; \* $p < 0.05$ ; \*\* $p < 0.01$ ; \*\*\* $p < 0.001$ ; \*\*\*\* $p < 0.0001$ . Scale bar: 10  $\mu$ m.

It is important to note that in this experiment, because of its higher surface expression, we used the deletion mutant SynDIG4 $\Delta$ 170–89-myc instead of the double point mutant AVPA-myc. It is possible that removal of 20 amino acids in the deletion mutant could disrupt an interaction with GluA2. Multiple proteomic studies did find copurification of SynDIG4 with GluA1 as well as GluA2 (Shanks et al., 2012; Schwenk et al., 2012; Chen et al., 2014). Interestingly, in native AMPAR complexes SynDIG4 associates at the interface of GluA1 and another AMPAR auxiliary factor cornichon-2 (Yu et al., 2021). A follow-up proteomics study did report select enrichment of SynDIG4 with GluA1 over GluA2 (Schwenk et al., 2014), consistent with the cryo-EM study. Furthermore, there is reduced extrasynaptic GluA1 and GluA2 in hippocampal neurons derived from SynDIG4 knockout (KO) mice compared with WT (Matt et al., 2018). Together, these data suggest that there is a specific interaction between SynDIG4 and GluA1 (either GluA1 homomers or GluA1/GluA2 heteromers). Additional experiments are needed to understand the relationship between  $\mu$ 2-dependent SynDIG4 trafficking and establishment of extra-synaptic pools of GluA1-containing AMPARs important for synaptic plasticity.

## Disruption of SynDIG interactions with $\mu$ 2 increase surface expression in cultured hippocampal neurons

In contrast to heterologous cells, we have found that surface expression of both WT SynDIG1 and SynDIG4 is higher in cultured hippocampal neurons. However, neurons did recapitulate the same general phenotype seen in heterologous cells; more specifically, that expression of  $\mu$ 2-binding deficient SynDIG mutants increases surface expression of SynDIG proteins. We found that expression of SynDIG1 $\Delta$ 161–76, in comparison to WT SynDIG1, significantly increases surface protein expression in cultured hippocampal neurons. We also observed a significant increase in the surface expression of the SynDIG4 mutant AVPA compared to WT SynDIG4. Intriguingly, higher surface expression of SynDIG4 did not disrupt PSD95 cluster size, though AVPA was found to be co-localized with a higher percentage of PSD95 compared to WT SynDIG4. In future studies, it will be of interest to utilize higher resolution imaging to investigate the sub-synaptic localization of SynDIG4 relative to PSD95 and AMPAR subunits. We have shown using brain fractionation techniques that SynDIG4 is de-enriched from the postsynaptic density (PSD) (Kirk et al., 2016). One possibility is that surface SynDIG4 could be localized extrasynaptically to stabilize pools of GluA1. However, given the role of SynDIG4 in LTD (Trojano-Rodriguez et al., 2019), another intriguing possibility is that SynDIG4 could be localized to endocytic zones (Blanpied et al., 2002; Lu et al., 2007; Petrini et al., 2009), where it could play a specialized role in endocytosis of GluA1-containing heteromers or GluA1 homomers (Sanderson et al., 2016; Sanderson et al., 2021; Sanderson et al., 2012).

We have also shown here that in addition to  $\mu$ 2, SynDIG4 will also co-immunoprecipitate with  $\mu$ 1a,  $\mu$ 3a and  $\mu$ 4 (Figure 1). These other AP

complexes are involved in a variety of intracellular trafficking events for other AMPAR auxiliary proteins (Guardia et al., 2018). For example, stargazin, an AMPAR auxiliary protein that regulates AMPAR diffusion between extra-synaptic and synaptic sites (Bats et al., 2007), has been shown to possess an endocytic signal capable of interacting with multiple  $\mu$ AP subunits. The region around this signal is differentially regulated by phosphorylation, influencing the binding affinity for different  $\mu$  subunits and, thus, changes the intracellular trafficking of stargazin and its cargo. The authors showed that mutations in stargazin that disrupt interactions with  $\mu$ 2 and  $\mu$ 3a ultimately impaired trafficking of AMPARs during LTD (Matsuda et al., 2013). However, it remains an open question if phosphorylation or other post-translational modifications affect  $\mu$ AP binding or SynDIG-mediated AMPAR localization important for synaptic function.

## SynDIG1 is enriched in the TGN and traffics to the plasma membrane and early endosomes in COS7 cells

We have shown that SynDIG1 interacts with  $\mu$ 2 through a noncanonical endocytic signal. The deletion mutant myc-SD1 $\Delta$ 161–76 does not bind  $\mu$ 2; whereas myc-SD1 $\Delta$ 161–72 does, suggesting that the critical amino acids could be FLMM (YXX $\phi$  replacing Y with F), which is not unprecedented (Al-Hasani et al., 2002; Hu et al., 2001). It is worth noting that the myc-SD1 $\Delta$ 161–72 construct expressed at a lower level than other constructs, making co-immunoprecipitation comparisons more challenging. Nonetheless, when normalized for the lower expression, the amount co-immunoprecipitated was comparable to WT (Figure 1C). To make matters more complicated, SynDIG2, which is highly similar to SynDIG1 in this region, does not bind  $\mu$ 2 nor any  $\mu$ AP subunit tested (Figure 1B). Further mutation analysis, including the construction of SynDIG1/SynDIG2 chimeras, will be helpful in clarifying these complications.

When we blocked protein translation with cycloheximide to investigate steady state localization, we observed that both SynDIG1 and SynDIG2 are localized to the Golgi apparatus, which had been noted previously for SynDIG2 (de Chaldée et al., 2006), and to early endosomes. We showed that both molecules are enriched at the TGN rather than the cis-Golgi (Figure 3). Deletions of roughly homologous portions of each protein (SynDIG1 $\Delta$ 161–76 and SynDIG2 $\Delta$ 135–55) resulted in increased surface labeling (Figure 2) and decreased overlap with the TGN marker Golgin-97 (Figure 3). Using an antibody feeding approach with a myc-SynDIG1-Flag construct, we observed internalized SynDIG1 signal that overlaps with Golgin-97 (Figure 3D).

Taken together, these data show that both SynDIG1 and SynDIG2 are similar in that they are localized to the TGN, that they are present in early endosomes, and that they can traffic to the plasma membrane. However, they appear to be endocytosed through different mechanisms: SynDIG1 interacts with  $\mu$ 2, whereas SynDIG2 does not. One alternative explanation is that either or both molecules could harbor a Golgi

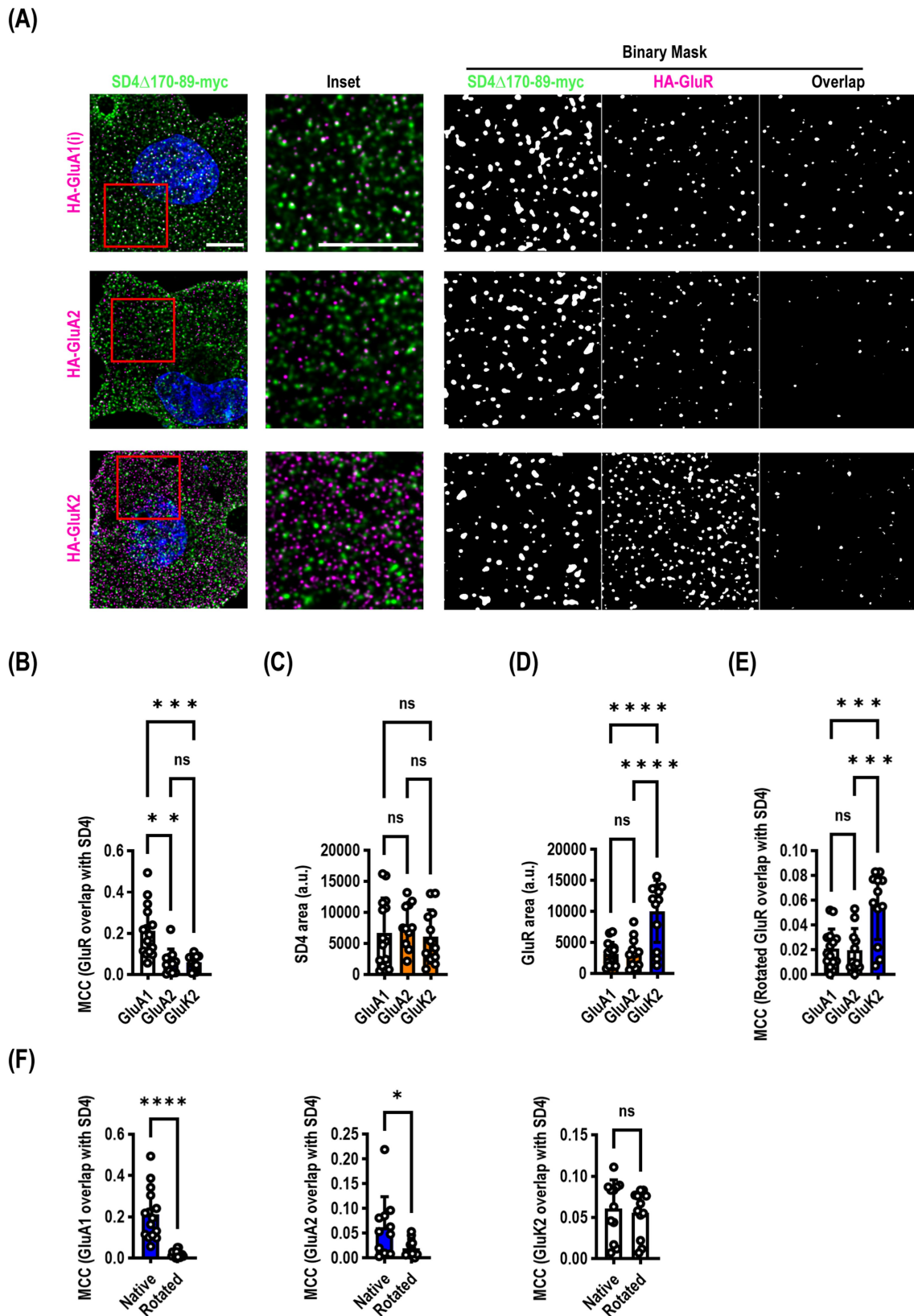


**FIGURE 4**  
 SynDIG4 can colocalize with GluA1 at the plasma membrane. COS7 cells were transiently transfected with SynDIG4 $\Delta$ 170–89-myc and HA-tagged ionotropic glutamate receptors and analyzed for colocalization of surface signal. (A) Representative images of SD4 $\Delta$ 170–89 colocalization with HA-GluA1, HA-GluA2 and HA-GluK2. (B) SynDIG4 colocalization with GluA1 is significantly greater than with GluA2 or GluK2. This is not due to differences in SynDIG4 expression (C) or increased GluA1 expression (D). As an additional control (E), to randomize the data, the SynDIG4 channel was rotated 90

(Continued)

FIGURE 4 (Continued)

degrees, and the Manders correlation coefficient (MCC) was recalculated. There was no difference between GluA1 and GluA2; however, the GluK2 MCC was significantly higher, likely due to the higher surface expression of GluK2. (F) There was a significant difference in the MCC between native and randomized data for GluA1 and GluA2, but not GluK2. Data are represented as mean  $\pm$  SEM;  $n = 11-15$  cells per group, each group from 2-3 independent experiments; ns not significant; \* $p < 0.05$ ; \*\* $p < 0.01$ ; \*\*\* $p < 0.001$ ; \*\*\*\* $p < 0.0001$ . Scale bar: 10  $\mu$ m.

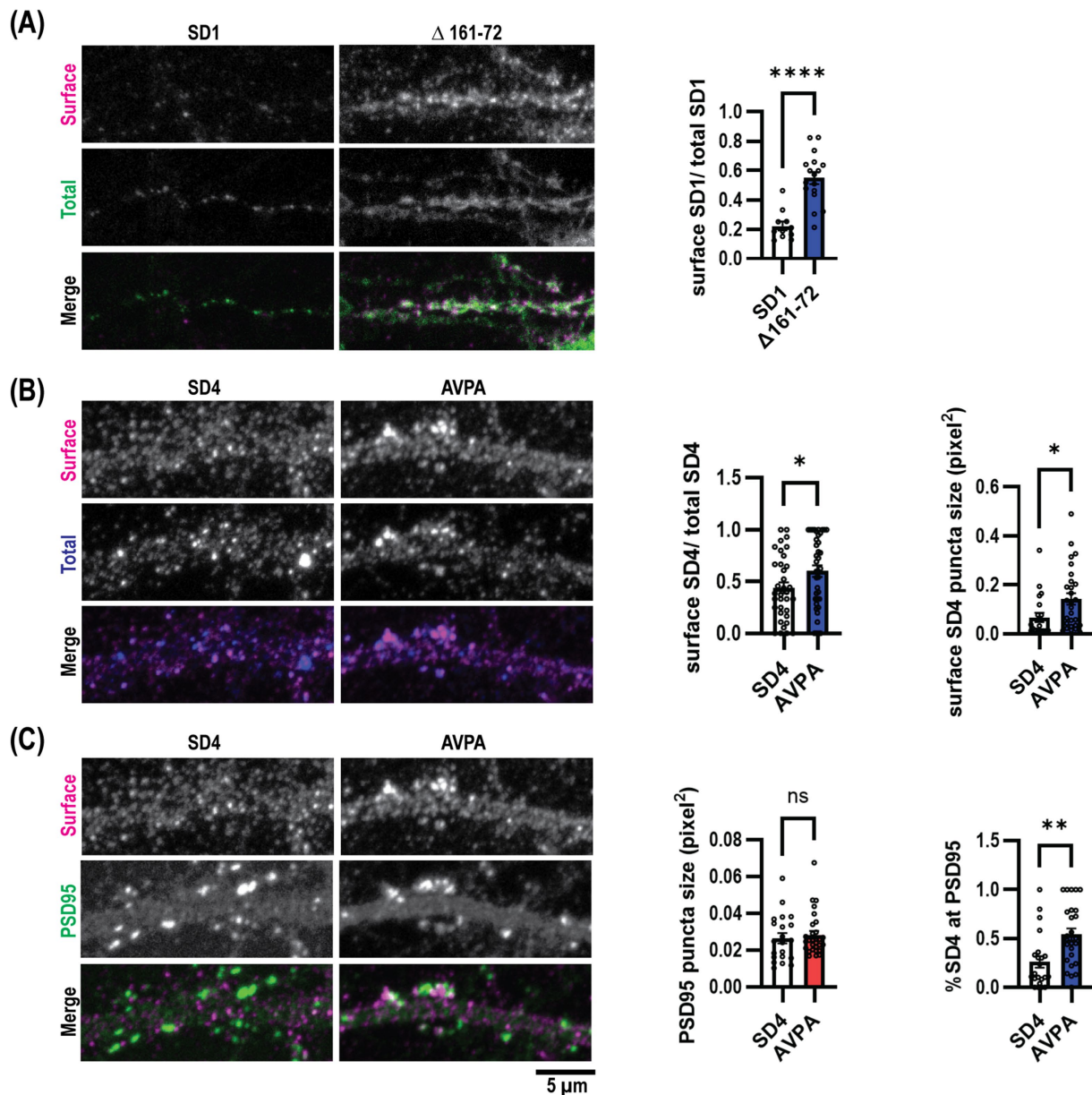


FIGURE 5

Endocytosis defective SynDIG mutations promote increased surface expression in cultured hippocampal neurons. Cultured hippocampal neurons were transfected and stained for surface and total SynDIG expression. (A) Representative dendrites with wild-type SynDIG1 and SynDIG1 $\Delta$ 161-76, and quantification of the ratio of surface-labeled to total-labeled SynDIG1 for wild-type and SynDIG1 $\Delta$ 161-76. (B) Representative dendrites with wild-type SynDIG4 and SynDIG4 AVPA, and quantification of the ratio of surface-labeled to total-labeled SynDIG4 for wild-type and AVPA. (C) Representative dendrites with wild-type SynDIG4 and SynDIG4 AVPA, and quantification of PSD95 puncta size and colocalization of surface SynDIG4 with PSD95 in wild type and AVPA transfected neurons. To determine the overlap with PSD95, the threshold for each independent experiment was determined by averaging the thresholds from at least 25% of the images. This average threshold was subsequently applied to all images for analysis. Colocalization of SynDIG4 and PSD95 was identified by using a PSD95 mask overlaid on SynDIG4 signals. The amount of SynDIG4 at PSD95 was quantified as the ratio of SynDIG4-PSD95 colocalized puncta to the total number of SD4 puncta. Data are represented as mean  $\pm$  SEM;  $n = 11-15$  cell per group, each group from 2 to 3 independent experiments; ns not significant; \* $p < 0.05$ ; \*\* $p < 0.01$ ; \*\*\* $p < 0.001$ ; \*\*\*\* $p < 0.0001$ . Scale bar: 5  $\mu$ m.

retention signal in the deleted region (Banfield, 2011), the removal of which could result in egress from the Golgi. For instance, disruption of a hypothetical Golgi retention signal in the SynDIG2Δ135–55 mutant, could explain the accumulation of this mutant on the plasma membrane without requiring disruption of a  $\mu 2$  binding interaction (Figure 2B).

We have also shown that SynDIG1 interacts with the  $\mu 1a$  subunit (Figure 1C). The AP1 complex can mediate both forward trafficking from the TGN to endosomes and retrograde transport of cargo from endosomes to the TGN (Guardia et al., 2018; Tu et al., 2020; Farias et al., 2014; Progida and Bakke, 2016). In this manner, SynDIG1 trafficking is similar to TGN38, an integral membrane protein that requires a YXX $\phi$  signal to cycle constitutively between the TGN and the plasma membrane (Roquemore and Banting, 1998). However, the possibility remains that even though SynDIG1 interacts with  $\mu 2$  and  $\mu 1a$ , some other molecular machinery which interacts with residues 161–76 could control trafficking to and from the TGN.

How might SynDIG1's localization and trafficking impact synapse development and plasticity? We speculate that SynDIG1 could be involved in sorting or trafficking of specific cargo in neurons during synapse development. In response to activity blockade, SynDIG1 might also alter trafficking of cargo, or posttranslational modifications such as palmitoylation could inhibit its interaction with AP2 and cause it to accumulate at the cell surface (Kaur et al., 2016) where it serves a direct role in synapse function. Future experiments are needed to address these questions regarding the intracellular trafficking of SynDIG1.

Taken together, our results provide insight into the mechanisms by which SynDIG proteins are targeted to intracellular compartments via an  $\mu$ AP-dependent manner. These foundational studies represent a first step in understanding SynDIG-mediated establishment of extra-synaptic pools of AMPARs important for synaptic plasticity. Many studies highlight the importance of dynamic AMPAR trafficking to and from synapses in the rapid modulation of synaptic strength during plasticity. Additional experiments in hippocampal neurons, including super-resolution and live-imaging approaches, are needed to expand upon these present results in the context of synaptic plasticity and are the focus of our current research efforts.

## Data availability statement

The raw data supporting the conclusions of this article will be made available by the authors, without undue reservation.

## Ethics statement

The animal study was approved by the UC Davis' IACUC (Institutional Animal Care and Use Committee). The study was conducted in accordance with the local legislation and institutional requirements.

## Author contributions

DS: Formal analysis, Methodology, Writing – original draft, Writing – review & editing, Investigation. C-WH: Formal analysis,

Investigation, Writing – review & editing. CM: Formal analysis, Investigation, Writing – review & editing. ES: Formal analysis, Investigation, Writing – review & editing. ED: Formal analysis, Writing – review & editing, Funding acquisition, Methodology, Writing – original draft.

## Funding

The author(s) declare that financial support was received for the research, authorship, and/or publication of this article. This work was supported by NIH grant #R01MH119347 (ED). CM was supported by the NIH T32 5T32MH112507–07.

## Acknowledgments

We are grateful to Dr. Juan Bonifacino (National Institutes of Health) for the  $\mu$ -3xHA constructs, to Dr. Yael Stern-Bach for HA-GluA1, HA-GluA2 and HA-GluK2 constructs, and to Dr. Jacob Yount (The Ohio State University College of Medicine) for the pCMV-myc-hIFITM3 (Addgene plasmid # 58461; <http://n2t.net/addgene:58461>; RRID:Addgene\_58461).

## Conflict of interest

The authors declare that the research was conducted in the absence of any commercial or financial relationships that could be construed as a potential conflict of interest.

The author ED declared that they were an editorial board member of Frontiers, at the time of submission. This had no impact on the peer review process and the final decision.

## Generative AI statement

The author(s) declare that no Generative AI was used in the creation of this manuscript.

## Publisher's note

All claims expressed in this article are solely those of the authors and do not necessarily represent those of their affiliated organizations, or those of the publisher, the editors and the reviewers. Any product that may be evaluated in this article, or claim that may be made by its manufacturer, is not guaranteed or endorsed by the publisher.

## Supplementary material

The Supplementary material for this article can be found online at: <https://www.frontiersin.org/articles/10.3389/fncel.2024.1526034/full#supplementary-material>

## References

- Al-Hasani, H., Kunamneni, R. K., Dawson, K., Hinck, C. S., Müller-Wieland, D., and Cushman, S. W. (2002). Roles of the N- and C-termini of GLUT4 in endocytosis. *J. Cell Sci.* 115, 131–140. doi: 10.1242/jcs.115.1.131
- Banfield, D. K. (2011). Mechanisms of protein retention in the Golgi. *Cold Spring Harb. Perspect. Biol.* 3:a005264. doi: 10.1101/cshperspect.a005264
- Bats, C., Groc, L., and Choquet, D. (2007). The interaction between Stargazin and PSD-95 regulates AMPA receptor surface trafficking. *Neuron* 53, 719–734. doi: 10.1016/j.neuron.2007.01.030
- Blanpied, T. A., Scott, D. B., and Ehlers, M. D. (2002). Dynamics and regulation of clathrin coats at specialized endocytic zones of dendrites and spines. *Neuron* 36, 435–449. doi: 10.1016/S0896-6273(02)00979-0
- Bonifacino, J. S., and Traub, L. M. (2003). Signals for sorting of transmembrane proteins to endosomes and lysosomes. *Annu. Rev. Biochem.* 72, 395–447. doi: 10.1146/annurev.biochem.72.121801.161800
- Chen, N., Pandya, N. J., Koopmans, F., Castelo-Székely, V., van der Schors, R. C., Smit, A. B., et al. (2014). Interaction proteomics reveals brain region-specific AMPA receptor complexes. *J. Proteome Res.* 13, 5695–5706. doi: 10.1021/pr500697b
- Chenau, G., Matt, L., Hill, T. C., Kaur, I., Liu, X. B., Kirk, L. M., et al. (2016). Loss of SynDIG1 reduces excitatory synapse maturation but not formation in vivo. *eNeuro* 3, ENEURO.0130-ENEURO16.2016. doi: 10.1523/ENEURO.0130-16.2016
- Chesarino, N. M., Compton, A. A., McMichael, T. M., Kenney, A. D., Zhang, L., Soewarna, V., et al. (2017). IFITM3 requires an amphipathic helix for antiviral activity. *EMBO Rep.* 18, 1740–1751. doi: 10.15252/embr.201744100
- Chesarino, N. M., McMichael, T. M., Hach, J. C., and Yount, J. S. (2014). Phosphorylation of the antiviral protein interferon-inducible transmembrane protein 3 (IFITM3) dually regulates its endocytosis and ubiquitination. *J. Biol. Chem.* 289, 11986–11992. doi: 10.1074/jbc.M114.557694
- Coomer, C. A., Rahman, K., and Compton, A. A. (2021). CD225 proteins: a family portrait of fusion regulators. *Trends Genet. TIG* 37, 406–410. doi: 10.1016/j.tig.2021.01.004
- de Chaldée, M., Brochier, C., Van de Vel, A., Caudy, N., Luthi-Carter, R., Gaillard, M. C., et al. (2006). Capucin: a novel striatal marker down-regulated in rodent models of Huntington disease. *Genomics* 87, 200–207. doi: 10.1016/j.ygeno.2005.10.009
- Desai, T. M., Marin, M., Chin, C. R., Savidis, G., Brass, A. L., and Melikyan, G. B. (2014). IFITM3 restricts influenza virus entry by blocking the formation of fusion pores following virus-endosome hemifusion. *PLoS Pathog.* 10:e1004048. doi: 10.1371/journal.ppat.1004048
- Díaz, E., Ge, Y., Yang, Y. H., Loh, K. C., Serafini, T. A., Okazaki, Y., et al. (2002). Molecular analysis of gene expression in the developing pontocerebellar projection system. *Neuron* 36, 417–434. doi: 10.1016/S0896-6273(02)01016-4
- Everitt, A. R., Clare, S., Pertel, T., John, S. P., Wash, R. S., Smith, S. E., et al. (2012). IFITM3 restricts the morbidity and mortality associated with influenza. *Nature* 484, 519–523. doi: 10.1038/nature10921
- Fariás, G. G., Gershlick, D. C., and Bonifacino, J. S. (2014). Going forward with retromer. *Dev. Cell* 29, 3–4. doi: 10.1016/j.devcel.2014.03.018
- Guardia, C. M., De Pace, R., Mattera, R., and Bonifacino, J. S. (2018). Neuronal functions of adaptor complexes involved in protein sorting. *Curr. Opin. Neurobiol.* 51, 103–110. doi: 10.1016/j.conb.2018.02.021
- Heldwein, E. E., Macia, E., Wang, J., Yin, H. L., Kirchhausen, T., and Harrison, S. C. (2004). Crystal structure of the clathrin adaptor protein 1 core. *Proc. Natl. Acad. Sci. USA* 101, 14108–14113. doi: 10.1073/pnas.0406102101
- Hu, W., Howard, M., and Lukacs, G. L. (2001). Multiple endocytic signals in the C-terminal tail of the cystic fibrosis transmembrane conductance regulator. *Biochem. J.* 354, 561–572. doi: 10.1042/bj3540561
- Jia, R., Xu, F., Qian, J., Yao, Y., Miao, C., Zheng, Y. M., et al. (2014). Identification of an endocytic signal essential for the antiviral action of IFITM3. *Cell. Microbiol.* 16, 1080–1093. doi: 10.1111/cmi.12262
- Kalashnikova, E., Lorca, R. A., Kaur, I., Barisoni, G. A., Li, B., Ishimaru, T., et al. (2010). SynDIG1: an activity-regulated, AMPA-receptor-interacting transmembrane protein that regulates excitatory synapse development. *Neuron* 65, 80–93. doi: 10.1016/j.neuron.2009.12.021
- Kaur, I., Yarov-Yarovoy, V., Kirk, L. M., Plambeck, K. E., Barragan, E. V., Ontiveros, E. S., et al. (2016). Activity-dependent Palmitoylation controls SynDIG1 stability, localization, and function. *J. Neurosci.* 36, 7562–7568. doi: 10.1523/JNEUROSCI.4859-14.2016
- Kirk, L. M., Ti, S. W., Bishop, H. I., Orozco-Llamas, M., Pham, M., Trimmer, J. S., et al. (2016). Distribution of the SynDIG4/proline-rich transmembrane protein 1 in rat brain. *J. Comp. Neurol.* 524, 2266–2280. doi: 10.1002/cne.23945
- Ling, S., Zhang, C., Wang, W., Cai, X., Yu, L., Wu, F., et al. (2016). Combined approaches of EPR and NMR illustrate only one transmembrane helix in the human IFITM3. *Sci. Rep.* 6:24029. doi: 10.1038/srep24029
- Lovero, K. L., Blankenship, S. M., Shi, Y., and Nicoll, R. A. (2013). SynDIG1 promotes excitatory synaptogenesis independent of AMPA receptor trafficking and biophysical regulation. *PLoS One* 8:e66171. doi: 10.1371/journal.pone.0066171
- Lu, J., Helton, T. D., Blanpied, T. A., Rácz, B., Newpher, T. M., Weinberg, R. J., et al. (2007). Postsynaptic positioning of endocytic zones and AMPA receptor cycling by physical coupling of dynamin-3 to Homer. *Neuron* 55, 874–889. doi: 10.1016/j.neuron.2007.06.041
- Martin, E. E., Wlekinski, E., Hoang, H. T. M., and Ahmad, M. (2021). Interaction and subcellular association of PRRT1/SynDIG4 with AMPA receptors. *Front. Synaptic Neurosci.* 13:705664. doi: 10.3389/fnsyn.2021.705664
- Matsuda, S., Kakegawa, W., Budisantoso, T., Nomura, T., Kohda, K., and Yuzaki, M. (2013). Stargazin regulates AMPA receptor trafficking through adaptor protein complexes during long-term depression. *Nat. Commun.* 4:2759. doi: 10.1038/ncomms3759
- Matt, L., Kirk, L. M., Chenau, G., Specca, D. J., Puhger, K. R., Pride, M. C., et al. (2018). SynDIG4/Prprt1 is required for excitatory synapse development and plasticity underlying cognitive function. *Cell Rep.* 22, 2246–2253. doi: 10.1016/j.celrep.2018.02.026
- Owen, D. J., and Evans, P. R. (1998). A structural explanation for the recognition of tyrosine-based endocytotic signals. *Science* 282, 1327–1332. doi: 10.1126/science.282.5392.1327
- Petrini, E. M., Lu, J., Cognet, L., Lounis, B., Ehlers, M. D., and Choquet, D. (2009). Endocytic trafficking and recycling maintain a pool of mobile surface AMPA receptors required for synaptic potentiation. *Neuron* 63, 92–105. doi: 10.1016/j.neuron.2009.05.025
- Plambeck, K. E., He, C. W., Navarro, H. H., and Díaz, E. (2022). Mutually dependent clustering of SynDIG4/PRRT1 and AMPA receptor subunits GluA1 and GluA2 in heterologous cells and primary neurons. *Front. Mol. Neurosci.* 15:788620. doi: 10.3389/fnmol.2022.788620
- Progida, C., and Bakke, O. (2016). Bidirectional traffic between the Golgi and the endosomes - machineries and regulation. *J. Cell Sci.* 129, 3971–3982. doi: 10.1242/jcs.185702
- Richter, K. N., Revelo, N. H., Seitz, K. J., Helm, M. S., Sarkar, D., Saleeb, R. S., et al. (2018). Glyoxal as an alternative fixative to formaldehyde in immunostaining and super-resolution microscopy. *EMBO J.* 37, 139–159. doi: 10.15252/embj.201695709
- Roquemore, E. P., and Banting, G. (1998). Efficient trafficking of TGN38 from the endosome to the trans-Golgi network requires a free hydroxyl group at position 331 in the cytosolic domain. *Mol. Biol. Cell* 9, 2125–2144. doi: 10.1091/mbc.9.8.2125
- Sällman Almén, M., Bringeland, N., Fredriksson, R., and Schiöth, H. B. (2012). The dispanins: a novel gene family of ancient origin that contains 14 human members. *PLoS One* 7:e31961. doi: 10.1371/journal.pone.0031961
- Sanderson, J. L., Freund, R. K., Gorski, J. A., and Dell'Acqua, M. L. (2021).  $\beta$ -Amyloid disruption of LTP/LTD balance is mediated by AKAP150-anchored PKA and Calcineurin regulation of Ca<sup>2+</sup>-permeable AMPA receptors. *Cell Rep.* 37:109786. doi: 10.1016/j.celrep.2021.109786
- Sanderson, J. L., Gorski, J. A., and Dell'Acqua, M. L. (2016). NMDA receptor-dependent LTD requires transient synaptic incorporation of Ca<sup>2+</sup>-permeable AMPARs mediated by AKAP150-anchored PKA and Calcineurin. *Neuron* 89, 1000–1015. doi: 10.1016/j.neuron.2016.01.043
- Sanderson, J. L., Gorski, J. A., Gibson, E. S., Lam, P., Freund, R. K., Chick, W. S., et al. (2012). AKAP150-anchored calcineurin regulates synaptic plasticity by limiting synaptic incorporation of Ca<sup>2+</sup>-permeable AMPA receptors. *J. Neurosci.* 32, 15036–15052. doi: 10.1523/JNEUROSCI.3326-12.2012
- Schwenk, J., Baehrens, D., Haupt, A., Bildl, W., Boudkazi, S., Roesper, J., et al. (2014). Regional diversity and developmental dynamics of the AMPA-receptor proteome in the mammalian brain. *Neuron* 84, 41–54. doi: 10.1016/j.neuron.2014.08.044
- Schwenk, J., Harmel, N., Brechet, A., Zolles, G., Berkefeld, H., Müller, C. S., et al. (2012). High-resolution proteomics unravel architecture and molecular diversity of native AMPA receptor complexes. *Neuron* 74, 621–633. doi: 10.1016/j.neuron.2012.03.034
- Shanks, N. F., Savas, J. N., Maruo, T., Cais, O., Hirao, A., Oe, S., et al. (2012). Differences in AMPA and kainate receptor interactomes facilitate identification of AMPA receptor auxiliary subunit GSG1L. *Cell Rep.* 1, 590–598. doi: 10.1016/j.celrep.2012.05.004
- Spence, J. S., He, R., Hoffmann, H. H., Das, T., Thion, E., Rice, C. M., et al. (2019). IFITM3 directly engages and shuttles incoming virus particles to lysosomes. *Nat. Chem. Biol.* 15, 259–268. doi: 10.1038/s41589-018-0213-2
- Troyano-Rodríguez, E., Mann, S., Ullah, R., and Ahmad, M. (2019). PRRT1 regulates basal and plasticity-induced AMPA receptor trafficking. *Mol. Cell. Neurosci.* 98, 155–163. doi: 10.1016/j.mcn.2019.06.008
- Tu, Y., Zhao, L., Billadeau, D. D., and Jia, D. (2020). Endosome-to-TGN trafficking: organelle-vesicle and organelle-organelle interactions. *Front. Cell Dev. Biol.* 8:163. doi: 10.3389/fcell.2020.00163

- Weston, S., Czieso, S., White, I. J., Smith, S. E., Kellam, P., and Marsh, M. (2014). A membrane topology model for human interferon inducible transmembrane protein 1. *PLoS One* 9:e104341. doi: 10.1371/journal.pone.0104341
- Wu, C. H., Tatavarty, V., Jean Beltran, P. M., Guerrero, A. A., Keshishian, H., Krug, K., et al. (2022). A bidirectional switch in the Shank3 phosphorylation state biases synapses toward up- or downscaling. *eLife* 11:e74277. doi: 10.7554/eLife.74277
- Yount, J. S., Karssemeijer, R. A., and Hang, H. C. (2012). S-palmitoylation and ubiquitination differentially regulate interferon-induced transmembrane protein 3 (IFITM3)-mediated resistance to influenza virus. *J. Biol. Chem.* 287, 19631–19641. doi: 10.1074/jbc.M112.362095
- Yount, J. S., Moltedo, B., Yang, Y. Y., Charron, G., Moran, T. M., López, C. B., et al. (2010). Palmitoylome profiling reveals S-palmitoylation-dependent antiviral activity of IFITM3. *Nat. Chem. Biol.* 6, 610–614. doi: 10.1038/nchembio.405
- Yu, J., Rao, P., Clark, S., Mitra, J., Ha, T., and Gouaux, E. (2021). Hippocampal AMPA receptor assemblies and mechanism of allosteric inhibition. *Nature* 594, 448–453. doi: 10.1038/s41586-021-03540-0
- Zhao, X., Li, J., Winkler, C. A., An, P., and Guo, J. T. (2018). IFITM genes, variants, and their roles in the control and pathogenesis of viral infections. *Front. Microbiol.* 9:3228. doi: 10.3389/fmicb.2018.03228